

Robust paramagnetism in $\text{Bi}_{2-x}\text{M}_x\text{Ru}_2\text{O}_7$ ($M = \text{Mn, Fe, Co, Ni, Cu}$) pyrochlore

M. K. Haas and R. J. Cava

Department of Chemistry and Princeton Materials Institute, Princeton University, Princeton, New Jersey 08540

M. Avdeev and J. D. Jorgensen

Argonne National Lab, Division of Materials Science, Argonne, Illinois 60439

(Received 8 May 2002; published 27 September 2002)

We report magnetic susceptibility, resistivity, and Seebeck coefficients for $\text{Bi}_{2-x}\text{M}_x\text{Ru}_2\text{O}_7$ pyrochlore. The solid solution exists up to $x = 0.5$ for $M = \text{Cu, Ni, Co}$ and up to $x = 0.1$ for $M = \text{Fe, Mn}$. The doped materials do not exhibit ferromagnetism or any localized ruthenium moment behavior. Instead we find the Ru-O and Bi-O sublattices to be essentially independent, with any magnetism resulting from the unpaired first-row transition metal dopant spins. Cobalt substitution for bismuth results in localized Co^{2+} and low-temperature spin-glass transitions in several cases. Nickel moments on the pyrochlore lattice display properties intermediate to localized and itinerant. Finally, copper doping results in an enhancement of the Pauli metallic density of states.

DOI: 10.1103/PhysRevB.66.094429

PACS number(s): 75.30.Cr, 61.72.Ww, 74.70.Pq

I. INTRODUCTION

Ruthenium-oxide-based perovskites are presently of great interest due to the range of magnetic and strongly correlated electronic behavior they exhibit, often breaching the limits of current condensed matter theory. Layered Sr_2RuO_4 , for example, is a superconductor at < 1 K and is postulated to have p -wave and spin-triplet pairing in the superconducting state.^{1,2} Of particular interest is the delicate balance many ruthenate perovskites display between ferromagnetism and exotic electronic states, and the sensitivity of the magnetic state to perturbation such as impurity concentration, applied field, or pressure. When superconducting Sr_2RuO_4 is doped by small amounts of nonmagnetic Ti^{4+} on the ruthenium site, there is a crossover from superconductivity to short-range ferromagnetic ordering.^{3,4} In the same structural system, $\text{Sr}_3\text{Ru}_2\text{O}_7$ shifts from a paramagnetic, strongly correlated Fermi liquid to a ferromagnet under applied pressure.⁵ Also, at fields above 7 T the compound undergoes a metamagnetic quantum transition to a high-moment state.⁶ Finally, Ti^{4+} doping on the ruthenium site of CaRuO_3 induces ferromagnetism in what was originally a paramagnetic material.⁷

The examples listed above are compounds based on the perovskite structure, and in fact much of the work in the ruthenate field centers on this structure type. Thus the question follows as to whether such ferromagnetic instabilities are found for other ruthenate classes. We investigate another common oxide structure, the pyrochlore. The pyrochlore oxide $\text{Bi}_2\text{Ru}_2\text{O}_7$, which exhibits temperature-independent Pauli paramagnetism and is weakly metallic, affords an excellent opportunity to test this generality.

Like the perovskite, the pyrochlore structure $A_2M_2O_7$ contains a three-dimensional network of corner-sharing MO_6 octahedra (Fig. 1). In the perovskite these are regular MO_6 octahedra with $160\text{--}180^\circ$ $M\text{-O-M}$ bonds, forming a three-dimensional square net of metal atoms. However, in the pyrochlore the corner-sharing results in tetrahedrally related metal atoms, and coordination is such that the $M\text{-O-M}$ bond angle must be $\sim 130^\circ$. The A cation in the pyrochlore occu-

pies hexagonal channels along $\langle 011 \rangle$ and equivalent directions, and three dimensionally the cations form an A_4O sublattice of corner-sharing tetrahedra.

Previous experimental work has probed differences between $\text{Bi}_2\text{Ru}_2\text{O}_7$, $\text{Y}_2\text{Ru}_2\text{O}_7$, and $\text{Ln}_2\text{Ru}_2\text{O}_7$, the latter two being electronically insulating although isoelectronic to $\text{Bi}_2\text{Ru}_2\text{O}_7$.⁸ One proposed reason for the difference is the change in Ru-O-Ru angle with A-cation size.^{9,10} It is also postulated that in the compounds $\text{Y}_2\text{Ru}_2\text{O}_7$ and $\text{Ln}_2\text{Ru}_2\text{O}_7$ the cation valence orbitals are energetically prohibited from contributing to Fermi level bonding, resulting in narrower localized bands.¹¹ Reports are conflicting as to whether bismuth s and p orbitals hybridize to some extent at the Fermi level, participating in conduction.^{12,13} Experimental work has followed the metal-insulator transition in several of these solid solutions.^{14,15} Here we report the properties of $\text{Bi}_{2-x}\text{M}_x\text{Ru}_2\text{O}_7$, $M = (\text{Mn, Fe, Co, Ni, Cu})$, observing that first-row transition metal d orbitals are proximate in energy to the Fermi level of $\text{Bi}_2\text{Ru}_2\text{O}_7$. Thus it is likely that the overall properties of these doped pyrochlores will be markedly different from those previously described in the literature.

II. EXPERIMENTAL METHODS

Suitable stoichiometric amounts of RuO_2 , Bi_2O_3 , Co_3O_4 , CuO , MnO_2 , Fe_2O_3 , and Ni_2O_3 were thoroughly mixed and

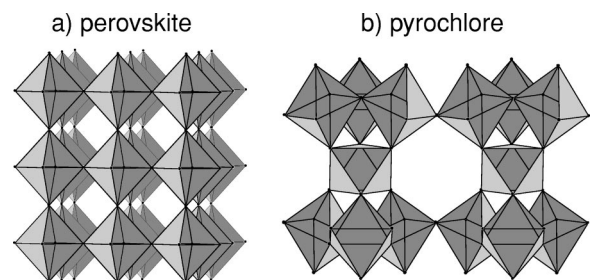


FIG. 1. View of RuO_6 network in (a) perovskite along $\langle 100 \rangle$ and (b) pyrochlore along $\langle 011 \rangle$.

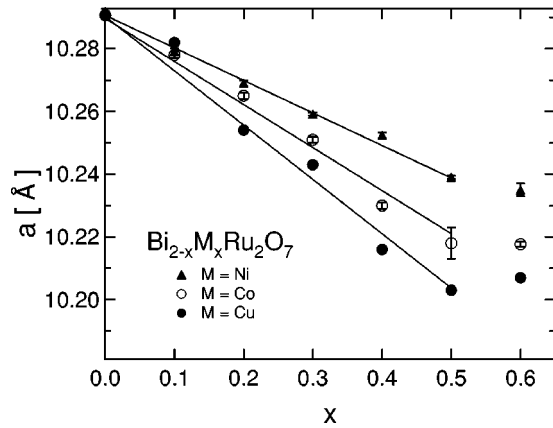


FIG. 2. Cubic lattice parameter of $\text{Bi}_{2-x}\text{M}_x\text{Ru}_2\text{O}_7$ as determined by powder x-ray diffraction vs doping level.

heated for several days between 750 and 1020 °C with intermediate grindings. Sample purity was monitored using room-temperature powder x-ray diffraction employing $\text{Cu K}\alpha$ radiation.

Magnetic properties and electrical resistivity were evaluated using a Quantum Design physical property measurement system (PPMS). For all samples, susceptibility was measured from 300 to 5 K in an applied field of 1 T. Data were also collected from 2 to 30 K in a field of 1 T after zero-field cooling, to assess any low-temperature magnetic transitions. Magnetic hysteresis loops were performed at 5 K in the range -9 to 9 T, and the data were fit to the paramagnetic Brillouin function $M = NgJ\mu_B B(x)$ where $x = m\mu_0 H/k_B T$.¹⁶ Resistivity measurements were performed on sintered powder pellets, which were cut into bars of approximately $1.5 \times 1.5 \times 3.5 \text{ mm}^3$, and measured with the standard four-point ac method. Seebeck coefficient measurements employed a commercial apparatus (MMR technologies).

III. RESULTS

Substitution of first-row transition metals on the ruthenium site of $\text{Bi}_2\text{Ru}_2\text{O}_7$ was not possible within the synthetic conditions explored. The metals Mn, Fe, Co, Ni, and Cu instead substitute on the bismuth site of the pyrochlore. We report complete structural characterization of $\text{Bi}_{1.6}\text{Cu}_{0.4}\text{Ru}_2\text{O}_7$, $\text{Bi}_{1.6}\text{Co}_{0.4}\text{Ru}_2\text{O}_7$, and $\text{Bi}_2\text{Ru}_2\text{O}_7$ elsewhere,¹⁷ by refinement of neutron powder diffraction data. This type of substitution is not unprecedented, as synthesis of $\text{Bi}_{2-x}\text{Cu}_x\text{Ir}_{2-y}\text{Ru}_y\text{O}_7$ was reported, although the compound was not fully characterized.¹⁸

Figure 2 plots lattice parameters obtained from powder x-ray diffraction as a function of x for $\text{Bi}_{2-x}\text{M}_x\text{Ru}_2\text{O}_7$ ($M = \text{Cu, Ni, Co}$). The lattice parameters decrease linearly to a first approximation. This is consistent with the smaller radii of the first-row transition metals in comparison to that of bismuth. For copper, nickel, and cobalt dopants, the solid solution exists up to $x = 0.5$: at larger nominal concentrations the lattice parameters remain relatively constant. In several samples, RuO_2 is found as a very minor impurity. As RuO_2

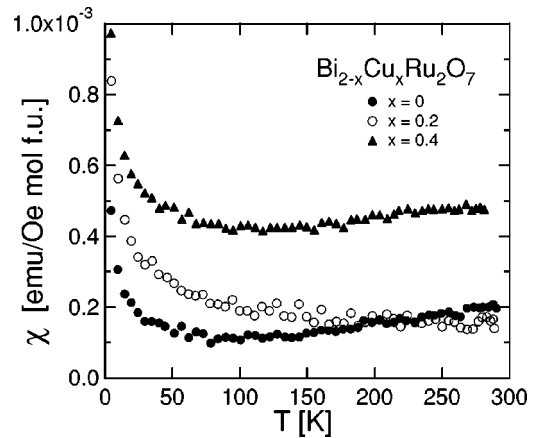


FIG. 3. Temperature-dependent magnetic susceptibility of $\text{Bi}_{2-x}\text{Cu}_x\text{Ru}_2\text{O}_7$.

is nonmagnetic and the amount present is negligible, its presence does not affect physical property characterization. For iron- and manganese-doped series the substitution limit is $x = 0.1$, resulting in unit cells of $a = 10.282(1)$ and $10.279(2)$, respectively.

A. $\text{Bi}_{2-x}\text{Cu}_x\text{Ru}_2\text{O}_7$

The magnetic susceptibility (χ) of $\text{Bi}_2\text{Ru}_2\text{O}_7$ between 300 and 5 K (Fig. 3) is essentially temperature independent. The relatively small susceptibility magnitude (2×10^{-4} emu/Oe mol f.u.) is consistent with Pauli paramagnetism. Also plotted in Fig. 3 are susceptibilities of $\text{Bi}_{1.6}\text{Cu}_{0.4}\text{Ru}_2\text{O}_7$ and $\text{Bi}_{1.8}\text{Cu}_{0.2}\text{Ru}_2\text{O}_7$. Twenty percent ($x = 0.4$) copper-doping increases the magnitude of χ by a factor of 2; likely due to an enhancement of the metallic density of states. There is no significant moment localization for either copper or ruthenium in these samples. Curie tails at low temperature are attributable to microscopic amounts of impurity spins.

Seebeck coefficients (S) for $\text{Bi}_{2-x}\text{Cu}_x\text{Ru}_2\text{O}_7$ are plotted in Fig. 4. (Small peaks around 300 K are instrumental.) Values of S for undoped $\text{Bi}_2\text{Ru}_2\text{O}_7$ are between -11 and

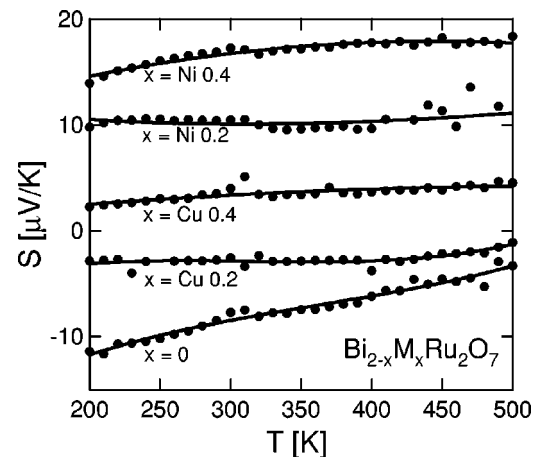


FIG. 4. Temperature-dependent Seebeck coefficients of $\text{Bi}_{2-x}\text{M}_x\text{Ru}_2\text{O}_7$ ($M = \text{Cu, Ni}$).

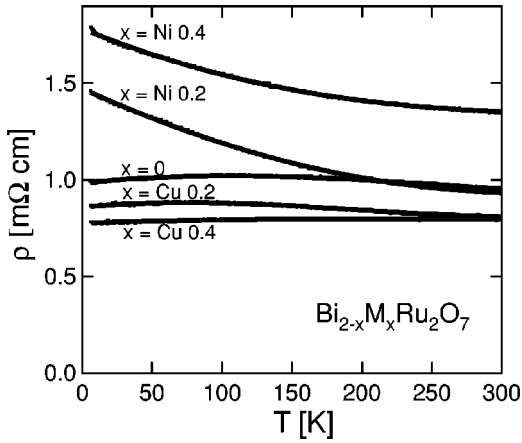


FIG. 5. Temperature-dependent resistivity of $\text{Bi}_{2-x}\text{M}_x\text{Ru}_2\text{O}_7$ ($M=\text{Cu}, \text{Ni}$).

$-4 \mu\text{V}/\text{K}$, indicating that the dominant carriers are electrons. Copper doping increases the magnitude of S : by 20% ($x=0.4$) substitution, S becomes positive and the dominant carriers cross over to hole-like.

Resistivity data are presented in Fig. 5. The resistivity of undoped $\text{Bi}_2\text{Ru}_2\text{O}_7$ is on the order of 1 m Ω cm, consistent with the description of a narrow band metal.¹⁹ The resistivity is largely temperature independent, unlike a typical good conductor where resistivity is expected to decrease more strongly with decreasing temperature. Copper doping slightly decreases the magnitude of the resistivity but maintains a similar temperature dependence compared to the undoped sample.

B. $\text{Bi}_{2-x}\text{Ni}_x\text{Ru}_2\text{O}_7$

Magnetic susceptibility data for nickel-substituted samples are shown in Fig. 6. The top panel plots measured susceptibility as a function of temperature. In contrast to copper doping, these samples display local moment behavior as nickel is substituted. By 20% ($x=0.4$) nickel doping, the magnetic susceptibility scales with the Curie-Weiss equation for localized paramagnetic moments. Data from nickel-doped samples for $x=0.3$ and $x=0.4$ were fit between 150 and 300 K to the function $\chi = \chi_0 + C/(T - \theta_{CW})$, where χ_0 is the sum of all temperature-independent terms. Values for the effective moment and Curie-Weiss temperature (θ_{CW}) were extracted, with the results summarized in Table I. Moments are between 2.1 and 2.3 μ_B/Ni , only slightly less than the theoretical spin-only value of 2.82 for Ni^{2+} . Therefore the observed moment is accounted for by the nickel dopant, and it is unlikely that any local moment has been induced at ruthenium centers. Further, values of θ_{CW} are very small, indicating weak coupling in all cases.

The bottom panel of Fig. 6 plots inverse magnetic susceptibility for the nickel-doped samples, with experimental points overlaid by Curie-Weiss fits (solid lines) for $x=0.3$ and $x=0.4$. The overlays highlight evident deviation from ideal behavior below 100 K for the two samples. In fact, at doping levels of $x=0.2$ and lower, deviation from linear be-

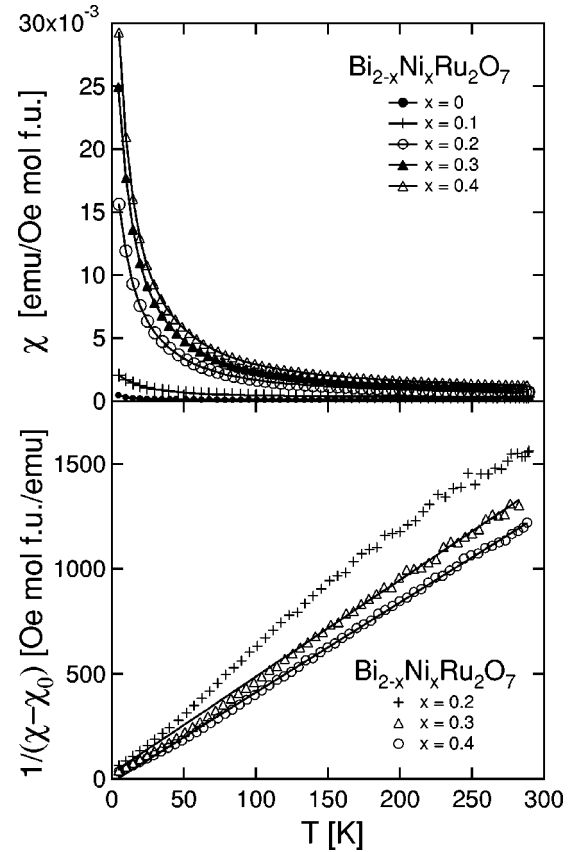


FIG. 6. Top panel: measured temperature-dependent magnetic susceptibility of $\text{Bi}_{2-x}\text{Ni}_x\text{Ru}_2\text{O}_7$. Bottom panel: inverse magnetic susceptibility (points) and Curie-Weiss fits (solid lines) for $\text{Bi}_{2-x}\text{Ni}_x\text{Ru}_2\text{O}_7$. Fitted temperature-independent terms (χ_0) are subtracted from measured χ in this panel.

havior is such that Curie-Weiss fitting is not applicable. Thus the magnetism can be classified as intermediate to localized and itinerant behavior.

Seebeck coefficients (S) for $\text{Bi}_{2-x}\text{Ni}_x\text{Ru}_2\text{O}_7$ are presented in Fig. 4. At 200 K, the magnitude of the coefficient ranges between $-10 \mu\text{V}/\text{K}$ for undoped $\text{Bi}_2\text{Ru}_2\text{O}_7$ and $+14 \mu\text{V}/\text{K}$ for $x=0.4$. Nickel-doped samples have higher values of S than do copper-doped samples, indicating that there exists a

TABLE I. Calculated magnetic constants from Curie-Weiss fitting.

Dopant x	χ_0 [emu/Oe mol f.u.]	θ_{CW} [K]	μ/μ_B [per x]
Ni 0.3	2.3×10^{-4}	-4.0(9)	2.39(1)
Ni 0.4	4.4×10^{-4}	3.7(6)	2.161(3)
Co 0.1	2.2×10^{-4}	1.3(3)	4.381(4)
Co 0.2	3.8×10^{-4}	2.1(3)	4.265(4)
Co 0.3	3.8×10^{-4}	1.9(5)	4.129(4)
Co 0.4	2.5×10^{-4}	2.1(2)	4.465(2)
Co 0.5	3.0×10^{-4}	-0.7(4)	4.269(2)
Fe 0.1	3.3×10^{-4}	0.1(3)	4.937(5)
Mn 0.1	1.6×10^{-4}	1.5(4)	5.112(6)

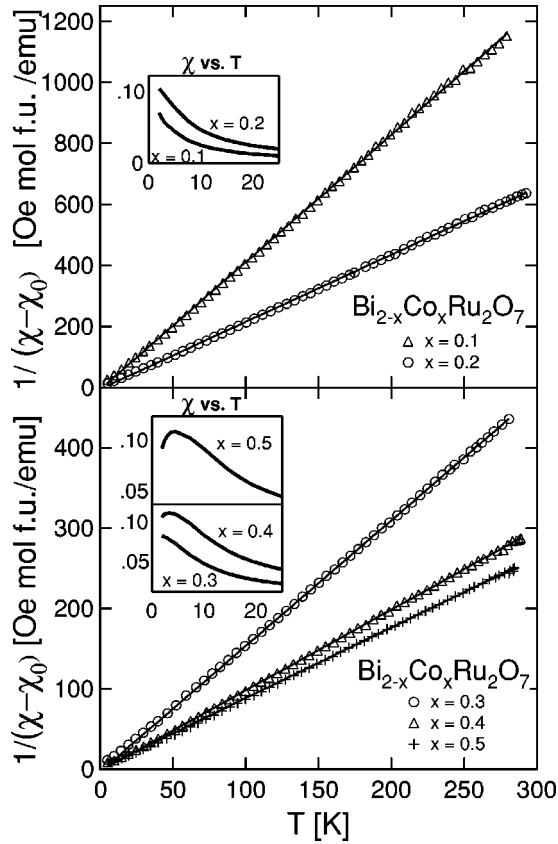


FIG. 7. Temperature-dependent inverse magnetic susceptibility (points) and Curie-Weiss fits (solid lines) for $\text{Bi}_{2-x}\text{Co}_x\text{Ru}_2\text{O}_7$. Fitted temperature-independent terms (χ_0) are subtracted from measured χ . Insets plot low-temperature magnetic susceptibility down to 2 K.

higher concentration of hole carriers in the latter. Resistivity (ρ) behavior is also different for the copper- and nickel-doped samples. Fig. 5 illustrates that while the former samples are less resistive than $\text{Bi}_2\text{Ru}_2\text{O}_7$, the latter samples are more resistive. As nickel is substituted on the lattice of $\text{Bi}_2\text{Ru}_2\text{O}_7$, the resistivity becomes more akin to that of a degenerate semiconductor, where ρ increases only slightly with decreasing temperature.

C. $\text{Bi}_{2-x}\text{Co}_x\text{Ru}_2\text{O}_7$

Cobalt doping has a dramatic effect on the magnetic properties of $\text{Bi}_2\text{Ru}_2\text{O}_7$. Samples of $\text{Bi}_{2-x}\text{Co}_x\text{Ru}_2\text{O}_7$ display Curie-Weiss behavior for $x=0.1-0.5$ in the temperature range 5–300 K. Plots of $1/(\chi - \chi_0)$ versus temperature (Fig. 7) demonstrate the goodness of fit, where calculated values (solid lines) overlay experimental points. The effective moment normalized to cobalt content (Table I) remains essentially constant across the doping series, indicating that the Curie moments are due solely to unpaired cobalt d electrons. Again no local moment is induced on ruthenium centers with doping. Calculated moments are between 4.1 and $4.4 \mu_B/\text{Co}$, which are slightly greater than the spin-only theoretical value of 3.87 for Co^{2+} but consistent with previously reported values for high spin Co^{2+} of

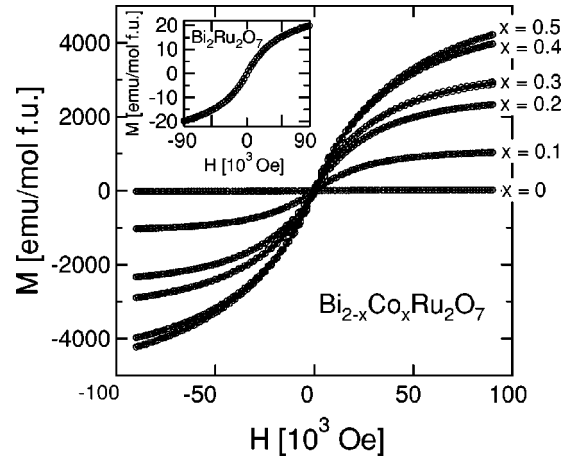


FIG. 8. Field-dependent magnetization of $\text{Bi}_{2-x}\text{Co}_x\text{Ru}_2\text{O}_7$. Inset: expansion of measured magnetization vs field data for undoped $\text{Bi}_2\text{Ru}_2\text{O}_7$ in the low-temperature region. Units in the inset are χ [emu/Oe mol f.u.], T [K].

$(4.1-5.2)\mu_B/\text{Co}$.²⁰ Values of θ are close to zero for all cobalt-doped samples, signifying that spin-coupling is very weak. Below 5 K, small peaks in magnetic susceptibility are observed for $x=0.4$ and $x=0.5$ samples, possibly due to spin-glass transitions (Fig. 7, inset). The fact that the transitions are at such low temperatures is consistent with weak coupling of the spins. Additionally, the peak maximum increases slightly from $x=0.4$ to $x=0.5$. And although there is not a distinct susceptibility peak for $x=0.3$, there are significant deviations from Curie-Weiss behavior below 5 K, signifying that some degree of spin interaction is also present at this doping level. The doped pyrochlores have the two characteristics common to spin-glass systems: atomic disorder and frustrated geometry.

Magnetization (M) versus field (H) data collected at 5 K (Fig. 8) for $\text{Bi}_{2-x}\text{Co}_x\text{Ru}_2\text{O}_7$ display no magnetic hysteresis at any doping level. The curves are not linear, but instead scale with the paramagnetic Brillouin function, as $m\mu_B H$ is on the order of $k_B T$ at this temperature and field range. Al-

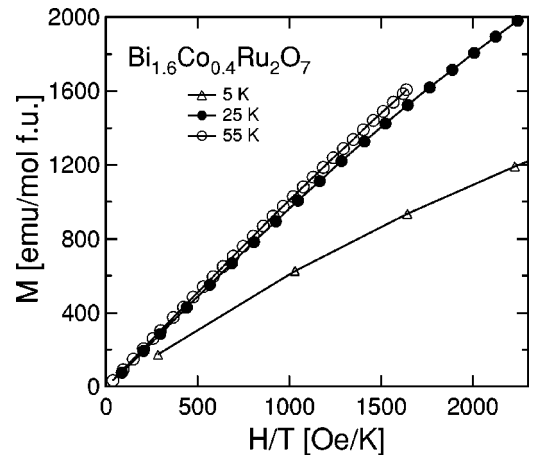


FIG. 9. Magnetization as a function of H/T for $\text{Bi}_{1.6}\text{Co}_{0.4}\text{Ru}_2\text{O}_7$, with data sets collected at three different temperatures.

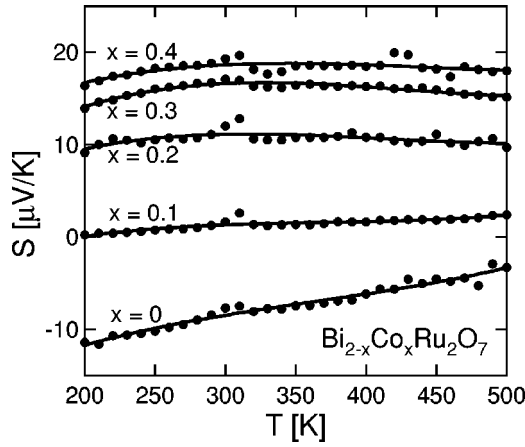


FIG. 10. Temperature-dependent Seebeck coefficients of $\text{Bi}_{2-x}\text{Co}_x\text{Ru}_2\text{O}_7$.

though M vs H for undoped $\text{Bi}_2\text{Ru}_2\text{O}_7$ does appear to be flat and linear at this scale, the figure inset shows the true shape of the curve. Fitting the high-field data for undoped $\text{Bi}_2\text{Ru}_2\text{O}_7$ to the Brillouin function with $g = 2$, the number of localized spin 1 moments is approximated to be 0.002 spins/mol f.u. For $\text{Bi}_{2-x}\text{Co}_x\text{Ru}_2\text{O}_7$ the magnetization increases with the amount of cobalt dopant as is expected. Figure 9 plots magnetization as a function of H/T for sample $\text{Bi}_{1.6}\text{Co}_{0.4}\text{Ru}_2\text{O}_7$. For noninteracting localized moments, data collected at different temperatures should superimpose, as is the case for plots at 25 and 55 K. However, data collected at 5 K deviate significantly, reflecting the interaction present between cobalt spins at this temperature. This is supported by our susceptibility data, where possible spin-glass ordering is present below 5 K for the more heavily doped samples. It is surprising that such a large number of magnetic Co^{2+} atoms are accommodated on the pyrochlore lattice without inducing magnetism on the ruthenium sublattice, and that the Co^{2+} spins are not more strongly interacting.

Seebeck coefficients (Fig. 10) increase with cobalt doping, once again hole-doping the pyrochlore. The slope of the temperature dependence of S also becomes flatter with increasing cobalt. The resistivity behavior of $\text{Bi}_{2-x}\text{Co}_x\text{Ru}_2\text{O}_7$ (Fig. 11) is similar to that of $\text{Bi}_{2-x}\text{Ni}_x\text{Ru}_2\text{O}_7$. As dopant is

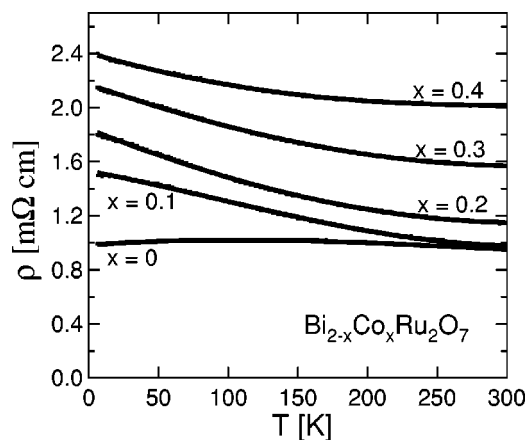


FIG. 11. Temperature-dependent resistivity of $\text{Bi}_{2-x}\text{Co}_x\text{Ru}_2\text{O}_7$.

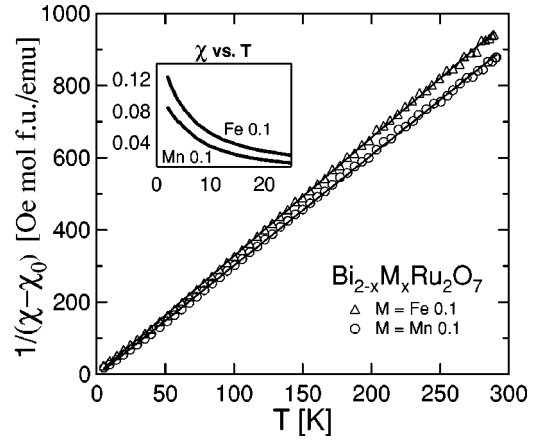


FIG. 12. Temperature-dependent inverse susceptibility (points) and Curie-Weiss fits (solid lines) for $\text{Bi}_{1.9}\text{Mn}_{0.1}\text{Ru}_2\text{O}_7$ and $\text{Bi}_{1.9}\text{Fe}_{0.1}\text{Ru}_2\text{O}_7$. Fitted temperature-independent terms (χ_0) are subtracted from measured χ . Inset plot measured magnetic susceptibility down to 2 K. Units for the inset are χ [emu/Oe mol f.u.], T [K].

introduced, the magnitude of the resistivity increases, and the temperature dependence becomes more semiconductor like. To examine the possibility of spin scattering as a mechanism for the increased resistivity, data were also collected for $\text{Bi}_{1.6}\text{Co}_{0.4}\text{Ru}_2\text{O}_7$ in an applied field of 9 T, which had no observable affect. Therefore spin scattering as a dominant mechanism is unlikely in these compounds, and the origin for the difference in resistivity trends between copper- and cobalt-doped samples remains unresolved.

D. $\text{Bi}_{1.9}\text{Fe}_{0.1}\text{Ru}_2\text{O}_7$ and $\text{Bi}_{1.9}\text{Mn}_{0.1}\text{Ru}_2\text{O}_7$

For dopants Fe and Mn, the substitution limit is 5% ($x = 0.1$). The susceptibilities for both $\text{Bi}_{1.9}\text{Fe}_{0.1}\text{Ru}_2\text{O}_7$ and $\text{Bi}_{1.9}\text{Mn}_{0.1}\text{Ru}_2\text{O}_7$ (Fig. 12) obey the Curie-Weiss law within the temperature range 5–300 K. Magnetic constants are listed in Table I. Fitted magnetic moments are $4.9 \mu_B/\text{Fe}$ and $5.1 \mu_B/\text{Mn}$, in good agreement with the spin-only theoretical value of $4.89 \mu_B$ when $S = 2$. The localized manganese spins are truly independent even down to low temperature, illustrated in Fig. 13 where magnetization is plotted as a function of field for $\text{Bi}_{1.9}\text{Mn}_{0.1}\text{Ru}_2\text{O}_7$. The high-field data are fit to the paramagnetic Brillouin function with set values $g = 2$ and $J = 2$, and with only N (number of spins per mole) allowed to vary. Assuming that all localized spins originate from manganese, the fit value of x for $\text{Bi}_{1.9}\text{Mn}_{0.1}\text{Ru}_2\text{O}_7$ is 0.10, in agreement with the nominal concentration. Resistivity and Seebeck coefficients data for Mn- and Fe-doped samples follow similar trends as those seen for Ni and Co, with the dopants once again increasing the magnitude of the resistivity and hole doping the pyrochlore. At 300 K, the magnitude of S is $2 \mu\text{V}/\text{K}$ for Mn ($x = 0.1$) and $-4 \mu\text{V}/\text{K}$ for Fe ($x = 0.1$).

IV. DISCUSSION

The pyrochlore structure can be described as two interpenetrating networks: one of corner-sharing RuO_6 polyhedra

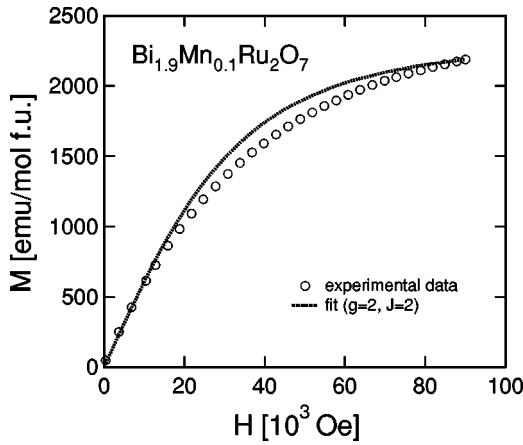


FIG. 13. Experimental magnetization vs field data for $\text{Bi}_{1.9}\text{Mn}_{0.1}\text{Ru}_2\text{O}_7$ and paramagnetic Brillouin function (dotted line).

and one of corner-sharing Bi_4O tetrahedra. Our magnetic data on transition metal doped $\text{Bi}_2\text{Ru}_2\text{O}_7$ indicates that the two networks are, surprisingly, magnetically independent.

We successfully substituted the first-row transition metal series Mn^{3+} , Fe^{2+} , Co^{2+} , Ni^{2+} , and Cu^{2+} on the bismuth site of $\text{Bi}_2\text{Ru}_2\text{O}_7$. Each of these dopants has unpaired valence-shell d electrons. However, the ruthenium moments in the pyrochlore are unaffected by Bi-site doping. This is in strong contrast to results for the doped perovskites $\text{CaRu}_{1-x}\text{Ti}_x\text{O}_3$ and $\text{Sr}_2\text{Ru}_{1-x}\text{Ti}_x\text{O}_4$. Although we find no ruthenium local moments, the unpaired dopant electrons diverge from localized to itinerant magnetic behavior across the first-row transition metal series. First, in $\text{Bi}_{1.9}\text{Mn}_{0.1}\text{Ru}_2\text{O}_7$ the substituted manganese moments are localized and essentially noninteracting, even down to low temperature. In $\text{Bi}_{2-x}\text{Co}_x\text{Ru}_2\text{O}_7$ the cobalt moments are also localized, with susceptibility data fitting the Curie-Weiss law between 5 and 300 K. However, at low temperature the spins are no longer completely isolated. In fact, spin-glass transitions are present below 5 K for $\text{Bi}_{1.6}\text{Co}_{0.4}\text{Ru}_2\text{O}_7$ and $\text{Bi}_{1.5}\text{Co}_{0.5}\text{Ru}_2\text{O}_7$. In nickel-doped samples the unpaired nickel spins display behavior intermediate to localized and itinerant. Finally, in copper-doped samples, there is no evidence for moment localization, and only the metallic temperature-independent paramagnetism is enhanced with doping. These magnetic trends are illustrated in Fig. 14, where the measured susceptibility at 5 K and 300 K is plotted as a function of dopant. For localized moments, the magnetic susceptibility at low temperature increases observably as a function of x , such as in the case of cobalt. However, for itinerant moments as in copper, $\chi_{5\text{K}}$ remains relatively flat with increasing x . For nickel, with atomic number intermediate to Co and Cu, the behavior is a combination of localized and itinerant. Up to $x=0.1$, $\chi_{5\text{K}}$ remains flat, while above $x=0.1$ it increases with x , although not as steeply as in the case of cobalt. Across the series, the d -orbitals of the first-row transition metal become more proximate in energy to the valance orbitals of oxygen. Thus copper hybridizes more strongly with oxygen than cobalt or nickel, resulting in itinerant behavior.

The transport properties of $\text{Bi}_{2-x}\text{M}_x\text{Ru}_2\text{O}_7$ are also

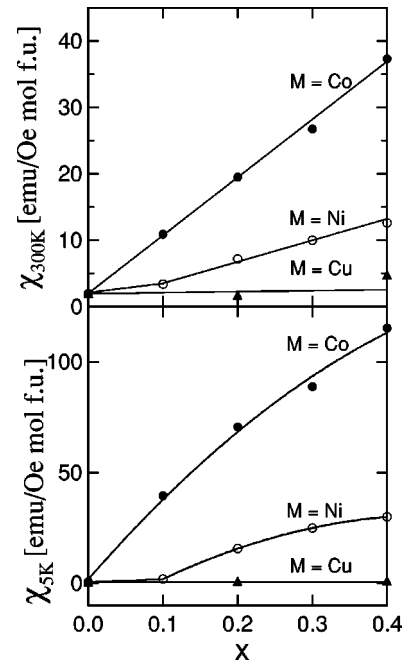


FIG. 14. Magnetic susceptibility at 300 K (top panel) and 5 K (bottom panel) as a function of dopant for copper- nickel-, and cobalt-doped samples.

evaluated. Figure 15 displays S as a function of dopant concentration for Co-, Ni-, and Cu-doped samples. At $x=0.4$, values of S are all positive. Thus in each series the dominant carriers cross over from electrons to holes upon doping. The absolute value of the Seebeck coefficient, $|S|$, is proportional to $\ln(N)-\ln(n)$ where n is the concentration of carriers and N the available density of states. If N is essentially constant, then copper doping results in an increased concentration of carriers (n) relative to undoped $\text{Bi}_2\text{Ru}_2\text{O}_7$. This interpretation agrees with resistivity data, where the magnitude of ρ decreases as copper is substituted on the pyrochlore lattice. Conversely, Seebeck coefficients for cobalt and nickel samples increase more steeply with x than those for copper. At $x=0.4$ for these two dopants, the concentration of carriers (n) is decreased relative to undoped $\text{Bi}_2\text{Ru}_2\text{O}_7$.

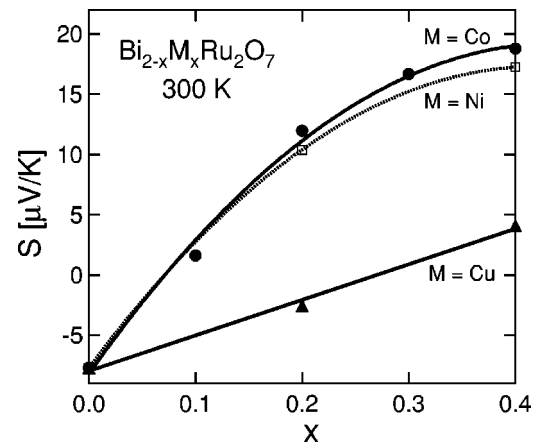


FIG. 15. Seebeck coefficients as a function of dopant concentration for copper-, nickel-, and cobalt-doped $\text{Bi}_2\text{Ru}_2\text{O}_7$.

V. CONCLUSION

In summary, we report magnetic and transport properties of $\text{Bi}_{2-x}\text{M}_x\text{Ru}_2\text{O}_7$ ($M = \text{Mn}, \text{Fe}, \text{Co}, \text{Ni}, \text{Cu}$). In no case did ferromagnetism or other localized ruthenium moment behavior occur upon doping. However, in such previously reported cases as $\text{CaRu}_{1-x}\text{Ti}_x\text{O}_3$ and $\text{Sr}_2\text{Ru}_{1-x}\text{Ti}_x\text{O}_4$, the dopant was substituted on the ruthenium site. Thus those substitutions could be expected to strongly perturb the Ru-O network. In the present study, the transition metal dopants preferentially replace bismuth in $\text{Bi}_2\text{Ru}_2\text{O}_7$. Our magnetic data indicate that the ruthenium and bismuth sublattices in $\text{Bi}_2\text{Ru}_2\text{O}_7$ are magnetically independent, and therefore the metal substitutions represent a second-order perturbation of the Ru-O lattice, which was not effective in causing a crossover to the

ferromagnetic state. In CaRuO_3 , conversely, A-site substitution does induce ferromagnetism even though it is not a direct perturbation of the Ru-O lattice.²¹ Therefore ruthenium oxides in the pyrochlore geometry appear to be far from the ferromagnetic instability observed in the perovskites, and such instability is not a broadly general characteristic of ruthenium oxide compounds.

ACKNOWLEDGMENTS

This work was supported by the National Science Foundation Grant No. DMR-9808941. The work at Argonne National Laboratory was supported by the U.S. Department of Energy, Office of Basic Energy Science, Contract No. W-31-109-ENG-38.

-
- ¹Y. Maeno, H. Hashimoto, K. Yoshida, S. Nishizaki, T. Fujita, J.G. Bednorz, and F. Lichtenberg, *Nature (London)* **372**, 532 (1994).
²Y. Maeno, T.M. Rice, and M. Sgrist, *Phys. Today* **54** (1), 42 (2001).
³M. Minakata and Y. Maeno, *Phys. Rev. B* **63**, 180504 (2001).
⁴K. Pucher, J. Hemberger, F. Mayr, V. Fritsch, A. Loidl, E.W. Scheidt, S. Klimm, R. Horny, S. Horn, S.G. Ebbinghaus, A. Reller, and R.J. Cava, *Phys. Rev. B* **65**, 104523 (2002).
⁵S.I. Ikeda, N. Shirakawa, S. Koiwai, A. Uchida, M. Kosaka, and Y. Uwatoko, *Physica C* **364-365**, 376 (2001).
⁶S.A. Grigera, R.S. Perry, A.J. Schofield, M. Chiao, S.R. Julian, G.G. Lonzarich, S.I. Ikeda, Y. Maeno, A.J. Millis, and A.P. Mackenzie, *Science* **294**, 329 (2001).
⁷T. He and R.J. Cava, *J. Phys. C* **13**, 8347 (2001).
⁸P. A. Cox, *Transition Metal Oxides* (Clarendon Press, Oxford, 1992).
⁹B.J. Kennedy, *Physica C* **241-242**, 303 (1998).
¹⁰K.S. Lee, D.K. Seo, and M.H. Whangbo, *J. Solid State Chem.* **131**, 405 (1997).
¹¹P. A. Cox, *The Electronic Structure and Chemistry of Solids* (Clarendon Press, Oxford, 1986).
¹²F. Ishii and T. Oguchi, *J. Phys. Soc. Jpn.* **69**, 526 (2000).
¹³W.Y. Hsu, R.V. Kasowski, T. Miller, and T.C. Chiang, *Appl. Phys. Lett.* **52**, 792 (1988).
¹⁴S. Yoshii, K. Murata, and M. Sato, *Physica B* **281-282**, 619 (2000).
¹⁵T. Yamamoto, R. Kanno, Y. Takeda, O. Yamamoto, Y. Kawamoto, and M. Takano, *J. Solid State Chem.* **109**, 372 (1994).
¹⁶L. Brillouin, *Phys. Radium* **8**, 74 (1927).
¹⁷M. Avdeev, M. K. Haas, J. D. Jorgensen, and R. J. Cava, *J. Solid State Chem.* (to be published).
¹⁸E. Beck and S. Kemmler-Sack, *Mater. Res. Bull.* **21**, 307 (1986).
¹⁹A. K. Cheetham and P. Day, *Solid State Chemistry Techniques* (Clarendon Press, Oxford, 1987).
²⁰K. Berger, *Coordination Chemistry: Experimental Methods* (Butterworths, London, 1973).
²¹T. He, Q. Huang, and R.J. Cava, *Phys. Rev. B* **63**, 024402 (2001).